The Hydrocarbon Mobility Evaluation of middle Eocene low Maturity Lacustrine Shale in the Bohai Bay Basin: Implications from NMR Analysis

Di Chen[1]; Xiongqi Pang[1*]; Guoyong Liu[2]; Fujie Jiang[1]; Liang Li[2]; Min Li[1]; Zhihong Pan[3]; Song Wu[1]; Xingang Zhang[1]; Zhi Xu[1]

[1] State Key Laboratory of Petroleum Resources and Prospecting, China University of Petroleum, Beijing 102249, China.

[2] PetroChina Jidong Oilfield Company, Tangshan 063004, China;

[3] Department of Physics, University of Alberta, Edmonton, AB T6G 2E1, Canada;

Corresponding author: Xiongqi Pang (pangxqcup@163.com) and Di Chen (cd18801323769@163.com)

Key Points:

- Low maturity brittle shale has low NMR porosity and oil saturation.
- NMR shows a promising mobility and potential of shale oil in MES shale.
- Bulk relaxation is more suitable for the micropore space in low maturity lacustrine shale.

Abstract

A vital factor influencing shale oil exploration in lacustrine shale reservoirs is oil mobility, which is closely associated with the shale pore structure and fluid properties, especially for the low-maturity lacustrine shale in China. In this study, the oil mobility and shale oil potential in the Middle Eocene Shahejie Formation lacustrine shale (MES shale) of the Nanpu Sag in the Bohai Bay Basin were evaluated by using nuclear magnetic resonance (NMR) experiments. The low-maturity MES shale has low porosity with various pore types including intergranular and dissolution pores and microcracks. Its pore space spans nano- to microscale with dominant mesopores. The portion promoting fluid flow is complex and has good self-similarity with high high fractal dimensions. The porosity is related to the thermal maturity, and a higher maturity facilitates pore space development. The oil saturation in low-maturity shale is lesser with low free hydrocarbon due to the low the maturity. Considering the high viscosity and the dead oil, the NMR relaxation mechanism in smaller pore space of low-maturity shale is proposed to bulk relaxation. The movable oil with a viscosity lower than 10 cp accounts consideble pore space in the MES shale. Its viscosity relates with TOC content and thermal maturity. Comparing with other shale oil producing areas, MES shale has similar geological conditions and good brittleness, which hints a suitable and promising shale oil potential at low tectonic position in the Nanpu Sag under the technologies of in situ conversion process and hydraulic fracturing.

1 Introduction

As the word energy demand increasing, shale oil resources attracts more and more attention (Ambrose et al., 2010; Clarkson et al., 2012; Jarvie 2012; Mastalerz et al., 2013;). The oil mobility is very critical for the assessment of shale oil resources and its development mode, especially for lacustrine shale oil resources (Akkutlu et al., 2017; Li et al., 2019a). While, most studies about oil mobility focus on the hydrocarbon in sandstone reservoir, rarely for the lacustrine shale. Shale oil exploration is hot in China, while its thermal maturity is commonly low (Li et al., 2018; Chen et al., 2019; Xie et al., 2019). The oil mobility in low maturity is really essential, while it has been rarely studied systematically.

The oil mobility in shale reservoirs is closely related to the composition of minerals and organic matter (OM), its complex pore structure, thermal maturity, liquid properties, formation pressure and temperature (Ross and Bustin, 2009; Clarkson et al., 2012; Akkutlu et al., 2017; Bustin et al., 20l8; Li et al., 2019a; 2019b). The methods mianly focus on molecular dynamics simulation, organic geochemistry, and nuclear magnetic resonance (NMR) (Straley et al., 1997; Coates et al., 1999; Yao et al., 2010; Firouzi et al., 2014; Li et al., 2019a; Zolfaghari et al., 2017; Chen et al., 2017; Akkutlu et al., 2017; Li et al., 2019d). Molecular dynamics simulation provides a microscopic theoretical research approach to simulate fluid molecule adsorption, flow and properties in porous materials (Mosher et al., 2013. Collell et al., 2014; Firouzi et al., 2014; Sharma et al., 2014). While, the simulated result is difficult to accord with the geological conditions, and it cost a lot for the equipment and times. The organic geochemistry methods evaluating liquid mobility in shale sediments rely on key geochemical parameters obtained from laboratory experiments (Xie et al., 2019; Li et al., 2019a; 2019b). Although the geochemical method could reflect the amount of movable liquids and is relatively reliable for evaluating shale oil resources, it could not present the state and distribution of liquids in the complex pore system intuitively and directly, and the method does not consider the underground liquid properties and conditions. NMR is a noninvasive technique that can provide information about the pore

structure, liquid properties, oil saturation, in situ fluid amount and interactions between pore fluids and rock (Coates et al., 1999; Mahrooqi et al., 2002). It has been widely used to characterize the pore structure and pore size distribution in shale sediments (Hodgkins and Howard, 1999; Coates et al., 1999; Cohaut et al., 2000; Yao et al., 2010; Hassan, 2012; Yao and Liu, 2012; Hinai et al., 2014; Liu et al., 2018). However, most NMR studies on fluid mobility were mainly conducted under water-saturated and fully centrifuged conditions for sandstone, which reflects water mobility but does not represent oil mobility directly due to its different physicochemical properties. Moreover, few NMR studies have been performed on determining the oil saturation and properties, as well as the oil distribution in shale sediments pore system. However, these are imperative for the further exploration of shale oil.

In this study, low-field NMR combined with microscopy observations and geochemical experiments were performed on the low-maturity Eocene lacustrine shale in the Nanpu Sag of the Bohai Bay Basin, with three objectives: 1) investigating the pore structure and pore size distribution in the Eocene lacustrine shale; 2) analyzing the oil properties and mobility in the low-maturity shale, and 3) estimating the shale oil potential in the Nanpu Sag.

2 Geological setting

The Bohai Bay Basin is a Mesozoic-Cenozoic oil-bearing rift basin on the eastern Asia continent and has produced plenty of oil/gas in the past decades (Fig. 1a; Allen et al., 1997). Massive terrestrial sediments cover the Mesozoic and pre-Mesozoic basement rocks of the Bohai Bay Basin (Fig. 1b; Dong et al., 2010). The increasing difficulty of conventional resource exploration and oil and gas demand in China, oblige the unconventional oil/gas resource exploration in the Bohai Bay Basin, especially for shale oil resources (Zou et al., 2018; Pu, 2019; Li et al., 2019a). To date, good shale oil occurrence have been discovered in Eocene shale sediments at the Bohai Bay Basin with high daily shale oil production, such as Zhanhua and Dongying Sags (Zou et al., 2018). Moreover, a breakthrough in shale oil exploration has been attained in the Cangdong Sag with industrial-scale shale oil flow (Pu, 2019). The Nanpu Sag adjoining with the Guandong, Zhanhua and Dongying Sags, has similar geological conditions, is an important hydrocarbon-producing sag in the Bohai Bay Basin (Fig. 1a; Dong et al., 2010). Constrained by the sea, deep shale oil resource exploration faces many difficulties in recent years. The Gaoliu area of Nanpu Sag has a suitable oil occurrence in the MES shale sediments. Although the MES shale is thin with relatively low thickness, but it is one of the most important source rocks in the Nanpu Sag, which contributed a large number of oil and gas (Chen et al., 2019). The MES shale was deposited in semi-deep and deep lacustrine environments and is dominated by black shale and gray-black mudstone, with abundant OM (Fig. 1b; Dong et al., 2010; Chen et al., 2019). MES shale is the typical low maturity lacustrine shale with a vitrinite reflectance of approximately 0.7% (Zheng et al., 2007; Chen et al., 2019). Although MES shale has a good hydrocarbon potential, few studies have been performed on the pore structure and oil mobility in the MES shale. Recently, well A1 in Gaoliu area were successfully drilled in a complete suite of MES shale sediments with good oil occurrence about 10 m. It is very encouraging, and enhances the confidence for the shale oil exploration in Nanpu sag. What's more, it is significant for shale oil exploration in the low maturity lacustrine shale. Therefore, the well A1 was continuous sampling, and a suite of MES shale samples were collected to analyze the pore structure and estimate the shale oil mobility, as well as their variation in vertical.

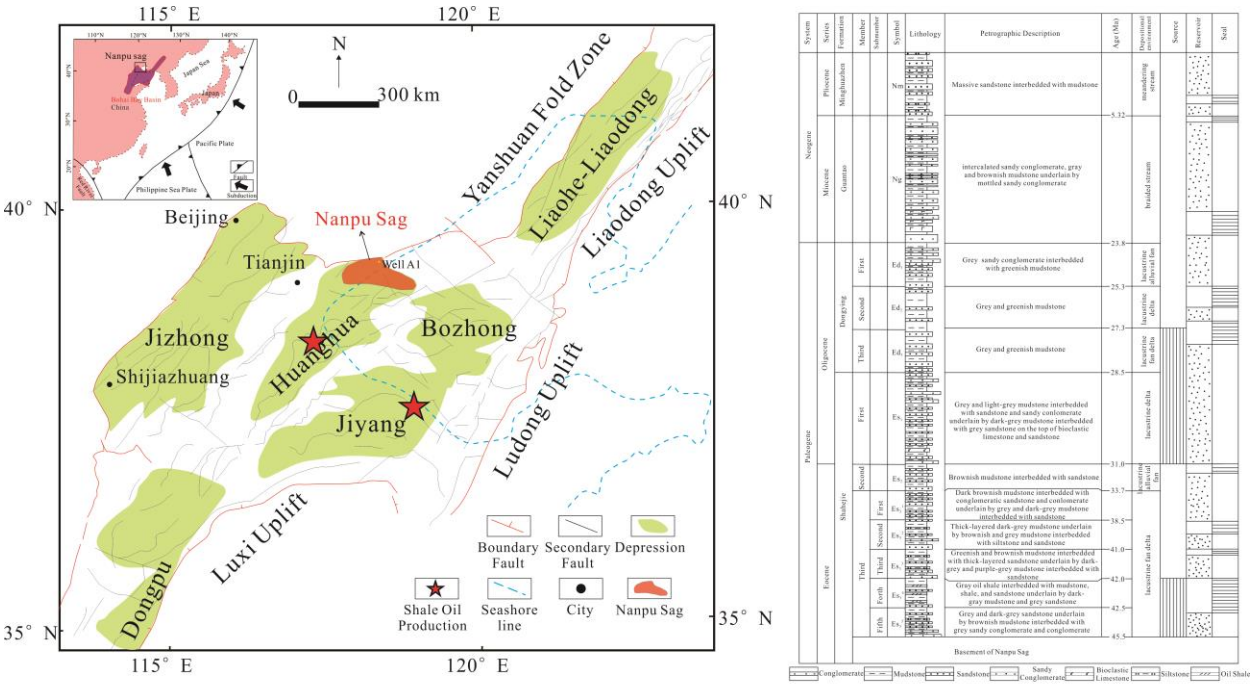

Figure 1. Geological location of Nanpu sag in the Bohai Bay Basin (a) and the stratigraphy distribution (b) modified from Dong et al. (2010) and Chen et al. (2019).

3 NMR Theory Background

NMR refers to the response of atomic nuclei to a magnetic field (Coates et al., 1999). Due to the net magnetic moment and angular momentum or spin, atomic nuclei, which have an odd number of protons or neutrons or both, proceed to spin under a given magnetic field and the gravitational field of Earth (Coates et al., 1999). When another external magnetic field is generated, the amplitude of these spinning magnetic nuclei will decay and produce irreversible rephrasing, thus inducing measurable resonant signals (Coates et al., 1999). The external magnetic field often uses the CPMG sequence (invented by Carr, Purcell, Meiboom and Gill; Coates et al., 1999), which will produce transverse magnetization decay signals with transverse relaxation time (T_2). Because the less time consuming, the T_2 transverse relaxation could be preferentially measured in the laboratory (Yao et al., 2010; Hinai et al., 2014; Liu et al., 2018).

For the transverse relaxation, three relaxation mechanisms occur for the fluids in rocks (Coates et al., 1999): (1) bulk relaxation in connection with the intrinsic fluid properties, (2) surface relaxation reflecting the characteristics of the interaction between fluids and the solid grain interfaces, and (3) diffusion relaxation induced by the gradient field. The relaxation processes mentioned above act in parallel, and their rates are additive. For a water-wet rock, the relaxation of water is dominated by the surface relaxation mechanism, while the relaxation of oil is dominated by bulk relaxation especially for the high viscosity oil and that in larger pore space or cracks (Coates et al., 1999). In contrast, the occurrences of oil and water will be reversed in a strongly oil-wet rock. Fine grains are significant barriers to diffusion, and diffusion relaxation would decrease under a low and uniform magnetic field (Kleinberg and Horsfield, 1990; Appel

et al., 1999; Coates et al., 1999; Yao et al., 2010). Therefore, for the water in water-wet rock under a homogenous magnetic field and the CPMG sequence, only surface relaxation should be considered.

For bulk relaxation mechanism, the oil T_2 relaxation time is associated with the temperature and fluid viscosity, and the relationship is as follows:

$$T_{2bulk} = 0.00713 \times \frac{T_k}{\eta} \quad (1),$$

where T_k is the Kelvin temperature (°K) and η is the viscosity (cp). For the surface relaxation mechanism, the relaxation time is the average relaxation time for the nuclei in all pores (Coates et al., 1999; Hodgkins et al., 1999). The nuclei in small pores more easily interact with the grain surface than those in larger pores. Therefore, a shorter relaxation time could reflect the smaller pores (Coates et al., 1999; Hodgkins et al., 1999). The rates of relaxation are generally related to surface relaxation and pore surface-to-volume ratio, and this relationship can be described as (Coates et al., 1999; Hodgkins et al., 1999):

$$\frac{1}{T_2} = \rho \frac{S}{V} \quad (2),$$

where T_2 is the transverse relaxation time resulting from surface relaxation (in seconds) and ρ is the surface relaxivity (in microns/second), which is related to the concentration of paramagnetic sites on pore walls and reflects the ability of pore walls to promote proton relaxation. S/V is the surface area-to-volume ratio (per micron). For simple shapes, the surface-to-volume ratio is 3/r, where r is the radius of the sphere (Coates et al., 1999). For complex shapes, a shape factor F_p will be used to describe the surface-to-volume ratio as (Liu et al., 2008):

$$\frac{S}{V} = \frac{F_p}{r} \quad (3),$$

then, the relationship between the pore size and NMR transverse relaxation time T_2 can be described as:

$$\mathrm{r} = \rho \times F_p \times T_2 \quad (4).$$

If the surface relaxivity can be determined, the NMR T_2 spectrum can be used to quantitatively characterize the pore size distribution in rocks. The surface relaxivity largely varies with the mineralogy (Kleinberg, 1996; Coates et al., 1999). Carbonate surfaces exhibit a lower surface relaxivity than that of quartz surfaces, and high-iron rocks have a higher surface relaxivity (Coates et al., 1999).

In addition to reflect pore information and provide an accurate estimate of the pore size distribution, NMR relaxation time distributions could also be used to analyze the oil information in porous media (Kleinberg and Vinegar, 1996; Coates et al., 1999; Mahrooqi et al., 2003). To characterize the oil saturation in cores containing oil and water, the signals produced by water need to be filtered out. Paramagnetic ions could cover the resonant signals from water (Kleinberg and Vinegar, 1996). If the manganese ion concentration is high enough, the T_2 of water could be reduced to below the dead time, and the water signal would disappear. However, manganese does not dissolve in hydrocarbons; therefore, T_2 from hydrocarbons is unaffected, and its signal remains. Fig. 2a shows that the signal intensity disappears when the concentration of manganese ions is higher than 10000 mg/L (Li et al., 2007). In addition, the signal intensity of the core

sample containing oil and water remains stable after immersion in a manganese solution with the same concentration for 18 hours (Fig. 2b; Li et al., 2007).

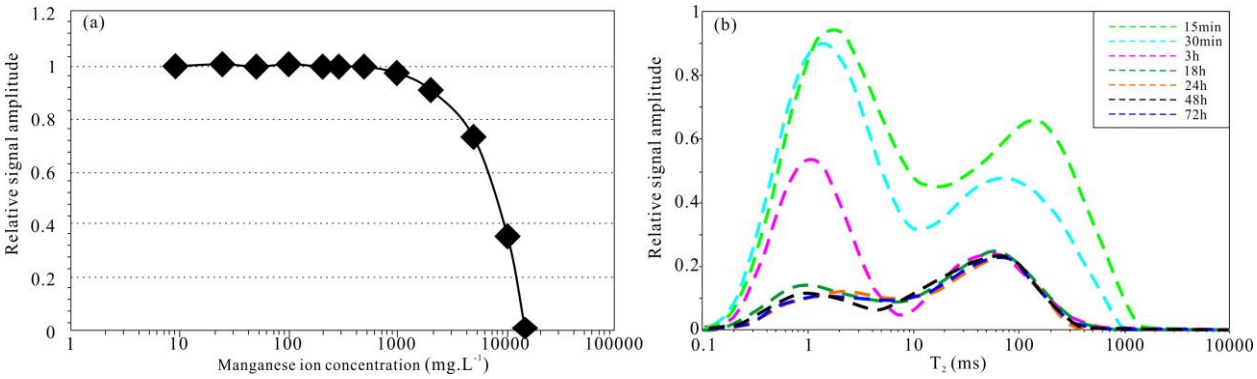

Figure 2. Shielding effect of manganese ion on the NMR signals (Li et al., 2007). (a) shows the better shielding effect with higher manganese ion concentration, and (b) indicates that the manganese has stable shielding effect on NMR signals after 18 hours for same concentration of manganese ion.

4 Sampling and methods

The sampling section of well A1 ranges from 3424.13 to 3472.83 m. The lithologies of the MES shale samples are mainly dark gray mudstone and gray oil shale and interbedded gray argillaceous siltstone. In this study, twenty-eight relatively good oil-bearing MES shale samples were collected to conduct NMR and scanning electron microscopy (SEM) experiments to analyze the mineral characteristics, pore structure, oil-bearing features and oil mobility.

Before the NMR experiments, horizontal cylindrical core plugs (2.5 cm in diameter and 4 cm length) were cut from the MES samples. All the MES shale samples in this study were subjected to two suites of NMR experiments. One suite was performed to obtain oil signals with which to characterize the oil-containing pore space. For this suite, all collected samples were immersed in a solution with a manganese ion concentration of 15000 mg/L and incubated for 24 hours to ensure that the water signal could be better suppressed. For the other suite of experiments, all core plugs were completely immersed in a 3% potassium chloride brine solution at 35 MPa under vacuum for 24 hours, to ensure that the samples were fully saturated with brine and reduce the sensitivity effect of clay minerals. This suite of experiments was executed to acquire the bulk signals corresponding to the bulk pore space.

The NMR measurements were performed with an AniMR-150 magnetic resonance imaging system at 35°C. The instrument contains a permanent magnet with a magnetic field strength of 0.3±0.05 T, and the resonance frequency is 2-30 MHz with an accuracy of 0.1 Hz. In this study, the CPMG sequence was applied in all corresponding experiments to obtain the distribution of the T_2 relaxation time. The measurement procedure settings were as follows: echo spacing, 0.1098 ms; echo number, 4096; scan number, 64. The decay signals were detected and disposed to T_2 distribution by using multiexponential fitted inversion (Coates et al., 1999). The signal intensity distribution of the T_2 relaxation time was obtained by using the echo data with preset times and plotted in logarithmic space from 0.01 ms to 10 s. If the samples were saturated enough, the pore space could be regarded as fully filled by brine or oil in the two sets experiments, and the measured magnitude of the transverse magnetization could reflect the brine

filled pore volume and oil filled pore volume respectively. In this study, the signal intensity was converted into the porosity through comparison with a preset standard sample by using the area proportion, and the details follows the experimental standard of SY/T 6490-2014. The bulk and oil-containing porosities were calculated according to the intensity of the brine and oil signals, respectively (Coates et al., 1999). The NMR results are presented as curves of the incremental and cumulative porosities with the T_2 relaxation time.

To further characterize the minerals and pore spaces, SEM analysis was performed on the MES samples. Fresh fracture surfaces were selected among the broken samples and coated with a thin gold layer. The prepared samples were examined with a ZEISS Crossbeam 540 scanning electron microscope equipped with an energy dispersive X-ray spectrometer. The mineral content in this study is based on a previous study Chen et al. (2019). All experiments in this study were performed at the State Key Laboratory of Petroleum Resources and Prospecting in China.

5 Results

5.1 Morphology of the MES Shale

The morphology of the pores and minerals in the MES shale are suitably characterized by SEM, as shown in Fig. 3. The SEM images reveal that the pore size in the MES shale ranges from 4 to 19 μm (Fig. 3a), and the pores exhibit lamellar structures that promote fluid flow. Pores are filled with granular pyrite, sheet-like mixed illite/smectite, and clean quartz (Fig. 3b). Abundant OM could be observed in SEM (Fig. 3c and 3e) surrounded by quartz, sheet-like illite and orthoclase (Fig. 3c). Cracks are observed in OM, which may be the result of hydrocarbon generation (Fig. 3e). Dissolution phenomena are observed on the particle surfaces of quartz, orthoclase, calcite, albite and ankerite, as shown in Fig. 3, indicating that the MES shale is in an acidic environment. The present pores include primary intergranular pores, intergranular and intragranular dissolution pores, microcracks in the OM, and micropores among the clay minerals.

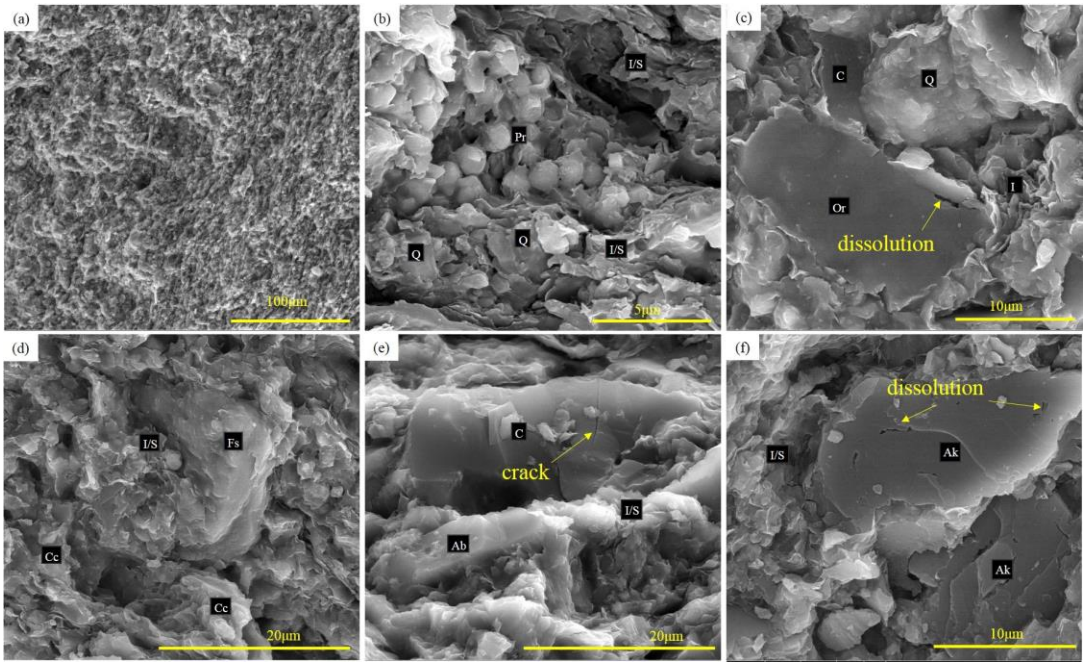

Figure 3. The morphological pictures from SEM observation for MES shale. Many minerals could be observed, including quartz (Q), pyrite (Pr), illite (I), illite/smectite mixture (I/S), orthoclase (Or), calcite (Cc), feldspar (Fs), albite (Ab), ankerite (Ak) and OM (C). Some cracks and dissolution could also been observed.

According to a previous study (Chen et al., 2019), the minerals in the MES shale are dominated by clays with an average content of 42.75%, followed by quartz ranging from 10-34% (avg. 21.73%) and calcite (2-39%, avg. 17.28%). In addition, gypsum, halite, anhydrite, pyrite and siderite were also detected in the MES shale. Furthermore, the brittleness index (BI) could be calculated to assess the mechanical fracturing. Considering the abundant OM and plastic clays in lacustrine shale, this study will calculate the BI by (Ma et al, 2019):

$$BI = (V_{felsic} + V_{carbonate})/(V_{clay} + V_{felsic} + V_{carbonate} + V_{organic}) \times 100 \quad (5),$$

where V_{felsic} is the felsic portion (%), and $V_{carbonate}$ is the carbonate portion (%), and V_{clay} is the clay portion (%), and $V_{organic}$ is the organic portion (%). When BI is > 40%, the rock will be brittle; when BI is > 60%, the rock is predicted to be highly brittle (Guo et al., 2015). The BI of MES shale ranges 37.73-79.36 (avg. 55.80, Fig. 4), indicating good brittleness. The BI of MES shale in Nanpu sag is higher than that of middle Jurassic Shimengou shale in the Qaidam Basin, but is slightly lower than that of Eocene shale sediments in Dongying sag (Fig. 4).

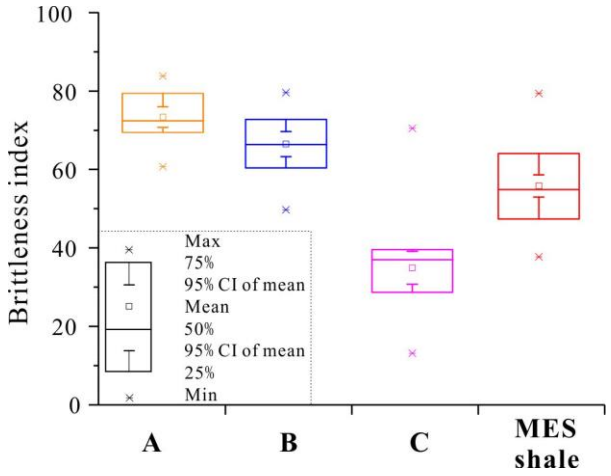

Figure 4. The BI comparison between MES shale and other lacustrine shale oil reservoir in China. A presents the Paleogene shale sediments in the Jiangsu Basin and Jiyang depression (Ma et al, 2019). B and C shows the Eocene shale sediments in Dongying sag (Zhang et al, 2019) and the middle Jurassic Shimengou shale in the Qaidam Basin (Hou et al, 2017), respectively.

251 **Table 1.** The information of MES shale and the parameters relating to NMR experiments.

Sample no.	Depth (m)	Surface relaxivity (μm/s)	T_{B1max} (ms)	T_{B2max} (ms)	T_{B0}	r_0 (nm)	T_{O1max} (ms)	T_{O2max} (ms)	T_{O0} (ms)	NMR porosity (%)	Oil saturation (%)	Porosity (<2nm, %)	Porosity (2-50nm, %)	Porosity (>50nm, %)
G-1	3424.13	41.29	0.24	11.61	1.60	198.61	0.21	7.71	2.96	5.57	14.78	0.06	4.00	1.51
G-2	3426.25	44.04	0.22	18.72	1.40	184.80	0.18	7.71	1.60	4.42	13.21	0.05	3.07	1.30
G-3	3426.62	74.57	0.24	14.25	1.40	312.91	0.19	8.25	2.59	4.29	12.65	0.04	2.29	1.95
G-4	3429.50	55.37	0.21	16.33	1.22	202.69	0.18	9.46	1.84	5.07	9.35	0.06	3.33	1.68
G-5	3431.37	40.39	0.22	14.25	1.60	194.28	0.19	8.84	2.26	4.86	15.50	0.06	3.69	1.12
G-6	3433.12	41.62	0.22	17.49	1.50	186.98	0.19	7.20	2.41	5.47	13.41	0.06	4.13	1.28
G-7	3435.24	68.37	0.21	16.33	1.22	250.28	0.18	8.25	1.06	4.80	12.15	0.06	2.50	2.24
G-8	3437.36	56.87	0.24	11.61	1.84	313.56	0.24	11.61	1.84	4.34	23.21	0.04	2.48	1.82
G-9	3439.61	51.47	0.22	16.33	1.40	215.98	0.19	10.13	1.22	4.99	12.73	0.04	3.35	1.60
G-10	3441.23	22.76	0.24	10.84	1.50	102.25	0.21	8.25	2.59	5.24	15.27	0.04	4.71	0.49
G-11	3443.23	22.76	0.21	12.43	1.31	89.20	0.16	7.71	1.40	4.82	12.97	0.06	4.36	0.40
G-12	3445.23	44.24	0.21	22.98	0.99	131.95	0.17	8.84	1.14	6.44	10.12	0.06	5.18	1.19
G-13	3447.23	58.77	0.25	10.84	2.41	425.79	0.25	10.84	2.41	5.11	30.19	0.06	2.63	2.43
G-14	3449.23	48.37	0.24	17.49	1.50	217.31	0.21	7.71	2.96	5.66	17.21	0.06	3.83	1.77
G-15	3451.22	49.02	0.38	14.25	1.72	252.45	0.22	7.20	4.46	6.46	19.88	0.06	4.07	2.33
G-16	3453.10	49.62	0.25	10.13	3.17	472.37	0.27	8.84	3.17	5.07	36.09	0.06	2.85	2.16
G-17	3455.10	54.02	0.22	21.46	1.31	211.72	0.16	6.72	1.50	7.34	10.36	0.06	4.89	2.39
G-18	3456.47	46.17	0.24	17.49	1.50	207.42	0.19	7.20	3.40	5.88	15.59	0.05	4.01	1.82
G-19	3459.47	53.92	0.21	18.72	1.14	184.36	0.18	8.84	1.22	5.85	10.67	0.06	4.06	1.74
G-20	3461.09	61.17	0.21	17.49	1.14	209.14	0.19	7.71	1.60	6.28	11.80	0.05	3.95	2.28
G-21	3462.96	47.59	0.22	13.31	1.84	262.40	0.22	8.25	6.28	5.88	19.23	0.05	3.78	2.05
G-22	3465.21	27.41	0.27	10.84	2.26	185.48	0.24	3.64	2.77	5.71	23.62	0.70	4.45	0.56
G-23	3466.21	102.32	0.25	11.61	2.26	692.39	0.22	6.28	2.77	5.50	16.37	0.05	1.66	3.80
G-24	3467.08	40.01	0.22	13.31	1.50	179.75	0.19	11.61	4.46	6.53	12.58	0.05	4.81	1.67
G-25	3468.46	61.92	0.24	15.26	1.60	297.84	0.21	4.46	7.20	5.81	14.20	0.06	3.33	2.42
G-26	3470.08	61.42	0.22	16.33	1.40	257.73	0.18	7.20	1.72	6.14	10.39	0.05	3.63	2.45
G-27	3471.33	62.52	0.22	17.49	1.31	245.03	0.19	7.20	1.60	7.42	9.95	0.06	4.58	2.78
G-28	3472.83	49.62	0.24	11.61	1.60	238.67	0.21	6.28	2.59	6.23	12.97	0.06	4.11	2.06

252

253 continued Table 1

Sample no.	Slope1	D_1	R^2	Slope2	D_2	R^2	Slope (>50nm)	$D_{(>50nm)}$	R^2
G-1	1.57	1.4264	0.85	0.01	2.9931	0.74	0.01	2.9867	0.51
G-2	1.66	1.3433	0.84	0.01	2.992	0.81	0.01	2.9876	0.58
G-3	1.70	1.2984	0.83	0.00	2.9951	0.80	0.02	2.9796	0.35
G-4	1.75	1.2532	0.85	0.01	2.9925	0.77	0.02	2.984	0.45
G-5	1.74	1.2614	0.78	0.01	2.9937	0.74	0.01	2.9879	0.50
G-6	1.73	1.2673	0.78	0.00	2.996	0.69	0.01	2.9904	0.39
G-7	1.71	1.2915	0.85	0.01	2.9908	0.78	0.02	2.9785	0.45
G-8	1.61	1.3914	0.82	0.01	2.9949	0.71	0.02	2.9782	0.40
G-9	1.76	1.2398	0.80	0.01	2.9941	0.71	0.01	2.994	0.73
G-10	1.64	1.3622	0.83	0.00	2.9962	0.61	0.00	2.9951	0.62
G-11	1.64	1.3605	0.82	0.01	2.9915	0.73	0.01	2.991	0.77
G-12	1.85	1.1487	0.82	0.01	2.9949	0.76	0.01	2.9917	0.50
G-13	1.66	1.3436	0.75	0.01	2.994	0.56	0.03	2.9738	0.42
G-14	1.70	1.3041	0.84	0.00	2.9964	0.68	0.01	2.9872	0.34
G-15	1.68	1.3195	0.81	0.01	2.9913	0.70	0.02	2.9802	0.49
G-16	1.81	1.1912	0.69	0.01	2.993	0.58	0.03	2.9739	0.48
G-17	1.91	1.0875	0.74	0.00	2.9968	0.72	0.01	2.9882	0.32
G-18	2.13	0.8742	0.73	0.01	2.9938	0.74	0.02	2.985	0.44
G-19	1.80	1.2011	0.84	0.01	2.9946	0.73	0.01	2.988	0.42
G-20	1.73	1.2737	0.86	0.00	2.9973	0.71	0.01	2.9872	0.29
G-21	1.38	1.6173	0.85	0.01	2.9929	0.68	0.02	2.981	0.45
G-22	1.49	1.5108	0.82	0.01	2.9889	0.67	0.02	2.9835	0.69
G-23	1.44	1.5592	0.84	0.01	2.9884	0.68	0.05	2.952	0.45
G-24	1.60	1.3955	0.85	0.01	2.9937	0.74	0.01	2.9881	0.51
G-25	1.57	1.4332	0.85	0.01	2.9943	0.75	0.02	2.9807	0.38
G-26	1.64	1.364	0.85	0.01	2.9913	0.78	0.02	2.9798	0.46
G-27	1.76	1.2397	0.84	0.01	2.994	0.81	0.02	2.982	0.38
G-28	1.65	1.3466	0.83	0.01	2.9944	0.72	0.02	2.9848	0.41

254

5.2 NMR T_2 Distribution

All 28 MES shale samples were subjected to NMR measurements under brine- and manganese- saturated conditions. The distributions of the measured bulk and oil porosities with the T_2 relaxation time, hereinafter referred to as BPD and OPD, respectively, are shown in Fig. 5a and 5b. The T_2 relaxation time of the MES shale ranges from 0.02 to 30.20 ms in both BPD and OPD, indicating a wide pore size distribution from small to large pores. All MES shale samples exhibit distinct bimodal distributions and contain two peaks for BPD and OPD, which suggests that the small and large pore systems are relatively independent in the MES shale. The bulk porosity is notably higher than the oil porosity for all MES shale samples. In this study, certain parameters are used to quantitatively characterize the distributions. As shown in Fig. 5a and 5b, T_{B1max} and T_{B2max} are the T_2 relaxation times at the first (P_{B1max}) and second (P_{B2max}) BPD peaks, respectively, and T_{O1max} and T_{O2max} are the same for OPD, which could reflect fluid properties such as the density and viscosity (Kleinberg and Vinegar, 1996; Coates et al., 1999). T_{B0} and T_{O0} are the final T_2 relaxation times of the first wave for BPD and OPD, respectively. T_{B0} could be regarded as the boundary between the movable and immovable fluids in this study according to the Coates-model (Hodgkins and Howard, 1999; Coates et al., 1999; Hinai et al. 2014). ΔT_{B1}, ΔT_{B2}, ΔT_{O1} and ΔT_{O2} are the difference T_2 values of half-peaks for BPD and OPD (Fig. 5a and 5b). The parameters of the 28 MES shale samples are summarized in Table 1.

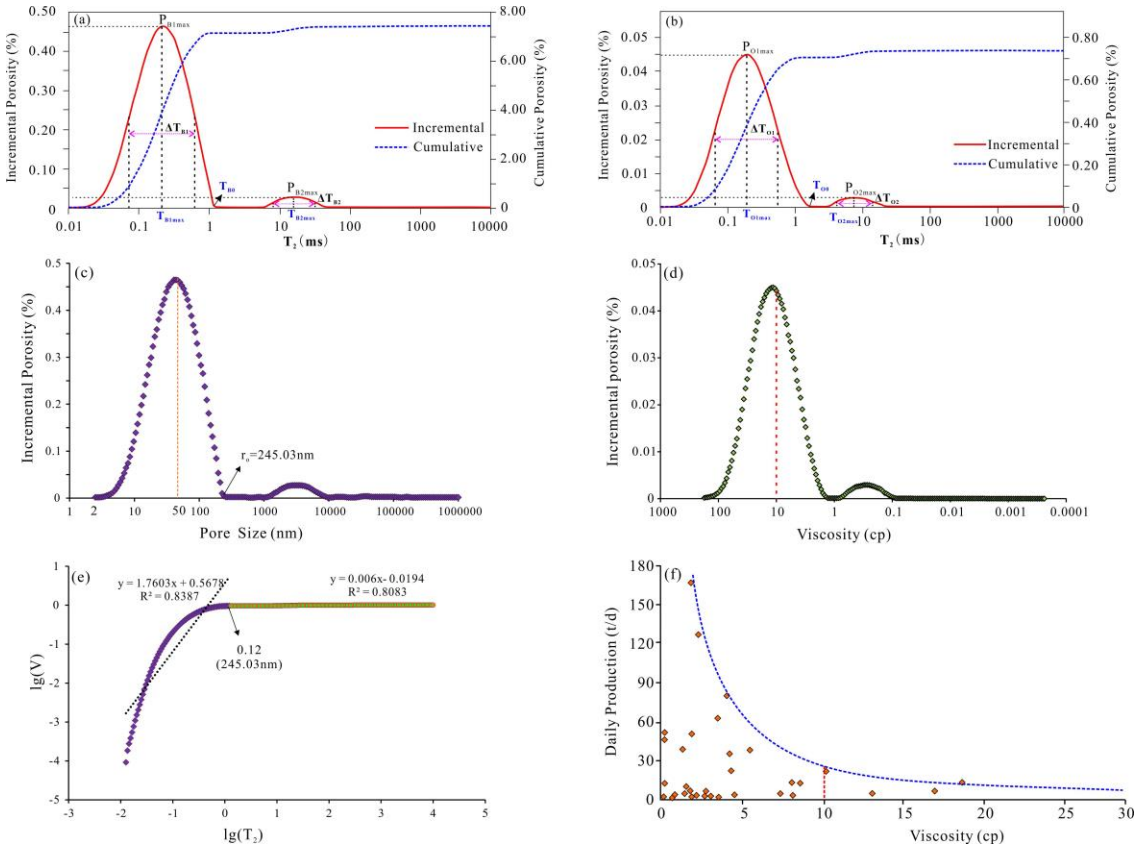

Figure 5. NMR T_2 Distributions of sample G-27. (a) shows the brine T_2 Distribution from brine saturated condition, and (b) shows the oil T_2 Distribution from manganese saturated condition. Other 27 samples show similar T_2 Distribution. The pore size distribution (c) and oil viscosity

distribution (d) of sample G-27 were obtained from T_2 Distribution. (d) shows the calculation of fractal dimension (d). Two suits of fractal dimensions could be discerned with a boundary at 245.03nm corresponding to the pore size boundary of immovable and movable fluids (r_0). (f) shows the relation of shale oil daily production and oil viscosity in Jiyang Depression (Chen et al., 2017). The red dotted lines in (d) and (f) show an oil viscosity of 10 cp. The oil viscosity less than 10cp has an acceptable daily production of shale oil in Dongying sag.

For most of the MES shale samples, T_{B1max} and T_{B2max} are slightly higher than T_{O1max} and T_{O2max}, respectively (Fig. 6a). The ΔT value exhibited no notable difference between BPD and OPD (Fig. 6b). The plot of the T_0 value shows two positive correlations between BPD and OPD for the MES shale samples (Fig. 6c). One positive correlation (yellow scatters in Fig. 6c) reveals a close relation for the T_0 values between BPD and OPD, while the other correlation (purple scatters in Fig. 6c) indicates a higher OPD T_0 value than BPD T_0 value. This feature reflects the difference between the boundaries of the movable and immovable fluids for the oil and brine in the MES shale. Three reasons may lead to this: 1) the complex pore systems and vertical anisotropy in the MES shale; 2) the large differences between the anisotropic fluid properties; and 3) the different relaxation mechanisms for the brine and oil. However, the proportion of immovable fluids is notably larger than that of movable fluids regardless of the oil or bulk liquids in the MES shale.

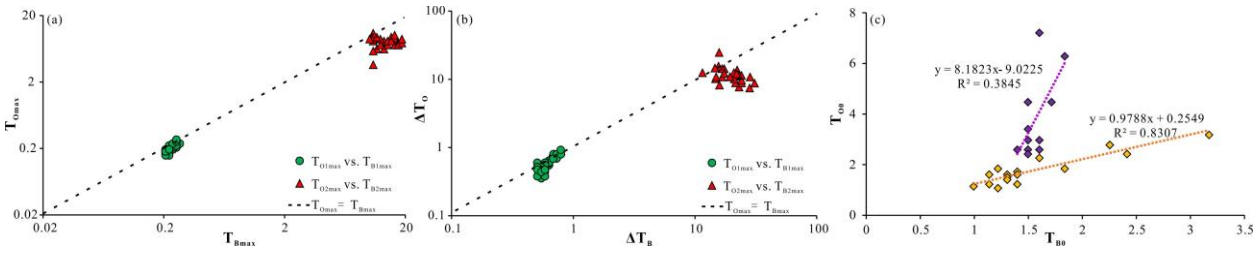

Figure 6. The plots of NMR T_2 distribution parameters used in this study for MES shale samples. T_{Omax} and T_{Bmax} is the T_2 relaxation time at peaks of brine and oil T_2 distributions respectively. ΔT_O and ΔT_B are the difference value of T_2 relaxation times at half of peaks of brine and oil T_2 distributions respectively. T_{B0} and T_{O0} are the end T_2 relaxation time of first wave at brine and oil T_2 distributions respectively.

5.3 Pore Size Distribution in the MES Shale

Equation (3) shows that the T_2 relaxation time can be converted into the pore size distribution if the shape factor and surface relaxivity can be determined. For the MES shale in this study, the pore shape could be regarded as a sphere and the value of F_p could be set as 3 with two reasons: 1) the clear bimodal T_2 relaxation distribution indicates two relatively independent pore systems coexisting in the MES shale, with a relatively low connectivity among pores; (2) the immovable fluids account for a larger percentage in the MES shale, also indicating a poor connectivity. The two reasons above suggest that there are very few pore throats in the MES shale and the pores are relatively isolated.

Previous studies show that the surface relaxivity is strongly associated with minerals (Kleinberg, 1996; Coates et al., 1999). Here, minerals were considered as the only effect factor of surface relaxivity, and a quantitative relation to calculate surface relaxivity was fitted by using multiple regression based on Liu's laboratory data which acquired from similar experimental conditions with this study (Liu et al., 2018). The relation could be expressed as:

$$\rho = 0.65 \times X_q + 1.80 \times X_f - 10.78 \times X_p + 0.95 \times X_c + 3.82 \quad (6),$$

where ρ is the surface relaxivity (nm/ms), and X_q, X_f, X_p and X_c are the contents of quartz, feldspar, pyrite and calcite (wt. %), respectively. The fitting parameters are shown in table 2. The significance F value of this regression is less than 0.01, and the low error, supporting the reliability of this relation. Afterwards, the surface relaxivity of the MES shale could be calculated according to the previous study (Table 1, Chen et al., 2019). The surface relaxivity of the MES shale ranges of 22.76-102.32 μm/s with an average value of 51.34 μm/s, which corresponds to the proposed 30-300 μm/s for clastics (Coates et al., 1999). Here, the pore size distribution of the brine-saturated MES shale samples could be obtained from T_2 relaxation time distribution, as shown in Fig. 5c. The dominant pore space size ranges from 2 to 260.53 nm, followed by a pore space size ranging of 0.75-3.95 μm. This pore size distribution means that the immovable fluid principally occurs in the nanoscale pore space and the movable fluid mainly distributing in the micron-sized pore space. Due to the water-wetting properties of the MES shale, the calculated surface relaxivity is only appropriate for brine; therefore, the oil-containing pore size could not be accurately obtained.

Table 2. The summary output of multiple regression.

Variables	Coefficients	standard error	t Stat	P-value	Lower 95%	Upper 95%
Intercept	3.82	1.12	3.41	0.08	-1.00	8.64
X_q	0.65	0.03	24.16	0.00	0.54	0.77
X_f	1.80	0.09	20.86	0.00	1.43	2.17
X_p	-10.78	0.25	-43.71	0.00	-11.84	-9.72
X_c	0.95	0.04	25.71	0.00	0.79	1.11
variance analysis						
	regression	SS: 538.86	MS: 134.71	F:1529.50	Significance F<0.001	
	residual	SS: 0.18	MS: 0.09			
regression statistics						
	R Square: 0.99	standard error: 0.30				

5.4 Porosity and Oil Saturation

As indicated in Table 1, the bulk porosity of the MES shale ranges from 4.29% to 7.41% with an average of 5.61%. The oil saturation ranges from 9.35%-36.09% with a mean of 15.59%, which is higher than that in the Dongying Sag at an oil saturation from 1%-8% (Chen et al., 2017). The pores could be divided into t micropores (<2 nm), mesopores (2-50 nm), and macropores (>50 nm) (Rouquerol et al., 1994). According to the calculated pore size distribution, the proportions of these three pore types can be obtained, as shown in Fig. 7. The pore space is dominated by mesopores ranging from 30.19%-90.43% (avg. 65.88%), followed by macropores

(2.26%-68.97%, avg. 32.74%). The micropores takes lowest percentage of 0.71%-12.22% (avg. 1.38%).

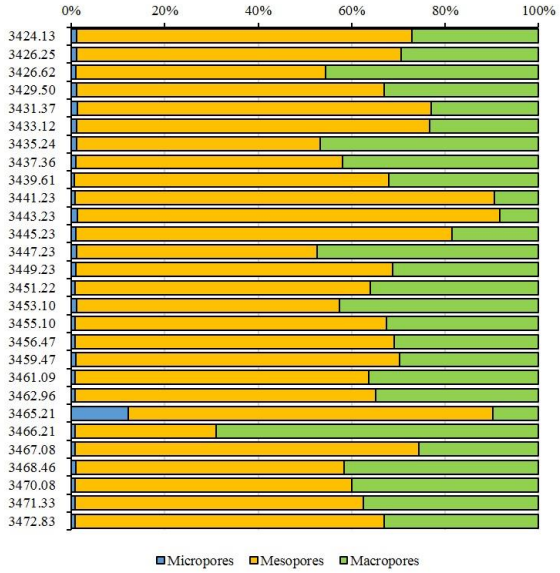

Figure 7. The percentage variations of micropores, mesopores and macropores in MES shale.

5.5 Fractal Characteristic

The T_2 relaxation reveals a complex pore structure in the MES shale. Furthermore, because the self-similarity requirement is satisfied for the geometry of complex rock pores, the degree of irregularity of the pore geometry could be quantitatively described by using fractal analysis with the fractal dimension (Hansen and Skjeltorp, 1988; Krohn, 1988; Jiang et al., 2016a). Based on the NMR T_2 relaxation, the fractal dimension could be calculated by (Shao et al., 2017):

$$\lg(\mathrm{V}) = (3 - \mathrm{D})\lg(T_2) + (\mathrm{D} - 3)\lg(T_{2max}) \quad (7),$$

where V is the cumulative pore volume fraction. Fractal dimension (D) ranges from 2 to 3, higher values indicates more complex and heterogenic pore space (Jiang et al., 2016a). It could be obtained from the slope of the plot of lg(V) versus lg(T_2) for each sample. For the brine-saturated samples, the fractal dimensions from NMR quantifies the complexity and heterogeneity of the pore structure. All MES shale samples show two distinct segments in the plots of lg(V) versus lg(T_2) that correspond perfectly to the immovable- and movable-fluid pore spaces, with a demarcation point of T_0, as shown in Fig. 5c. Therefore, the complexity of the immovable and movable fluid pore spaces could be quantified by using fractal dimensions D_1 and D_2 respectively. For MES shale, the D_1 value ranges from 1.0875 to 1.6173 except for an anomalous low value of 0.8742 in sample G-27, while the D_2 value varies of 2.9844-2.9973 (Table 1). Due to D ranging 2-3, all D_1 value are less than 2, thus it is invalid (Jiang et al., 2016a). This hints that the immovable pore spaces has weak self-similarity, and the description in the study of Shao et al. (2017) is unseemly. All D_2 value almost close to 3, indicating more complex pore system and self-similarity for the movable pore space. This phenomenon may be caused by the pore throats, which is an important factor controlling the fractal dimension and promote fluid flow (Jiang et al., 2016a). For the isolated pores, the fractal dimension would not be closely related to

its size due to its self-similarity. However, throats would connect the isolated pores and make the pore structure more complex, which would lead to a higher D value. In addition, the pore size distributions of immovable and movable pore space in Fig. 5c support a higher connectivity between the large pore spaces with high D values. For the large pore spaces, the r_0 and P_{B2max} values have clear negative correlations with the D_2 value (Fig. 8a and 8b). This means that the more complex pore structure system will lead to a lower pore size boundary for fluid flow under the throats effect to a great extent. Furthermore, the fractal dimensions of the macropores ($D_{>50nm}$) were also calculated as listed in Table 1, and the $D_{>50nm}$ value is generally lower than the D_2 value. This implies that the movable pore space is more complex, further supporting that the throats in porous media enhance its complexity and heterogeneity but promote liquid flow.

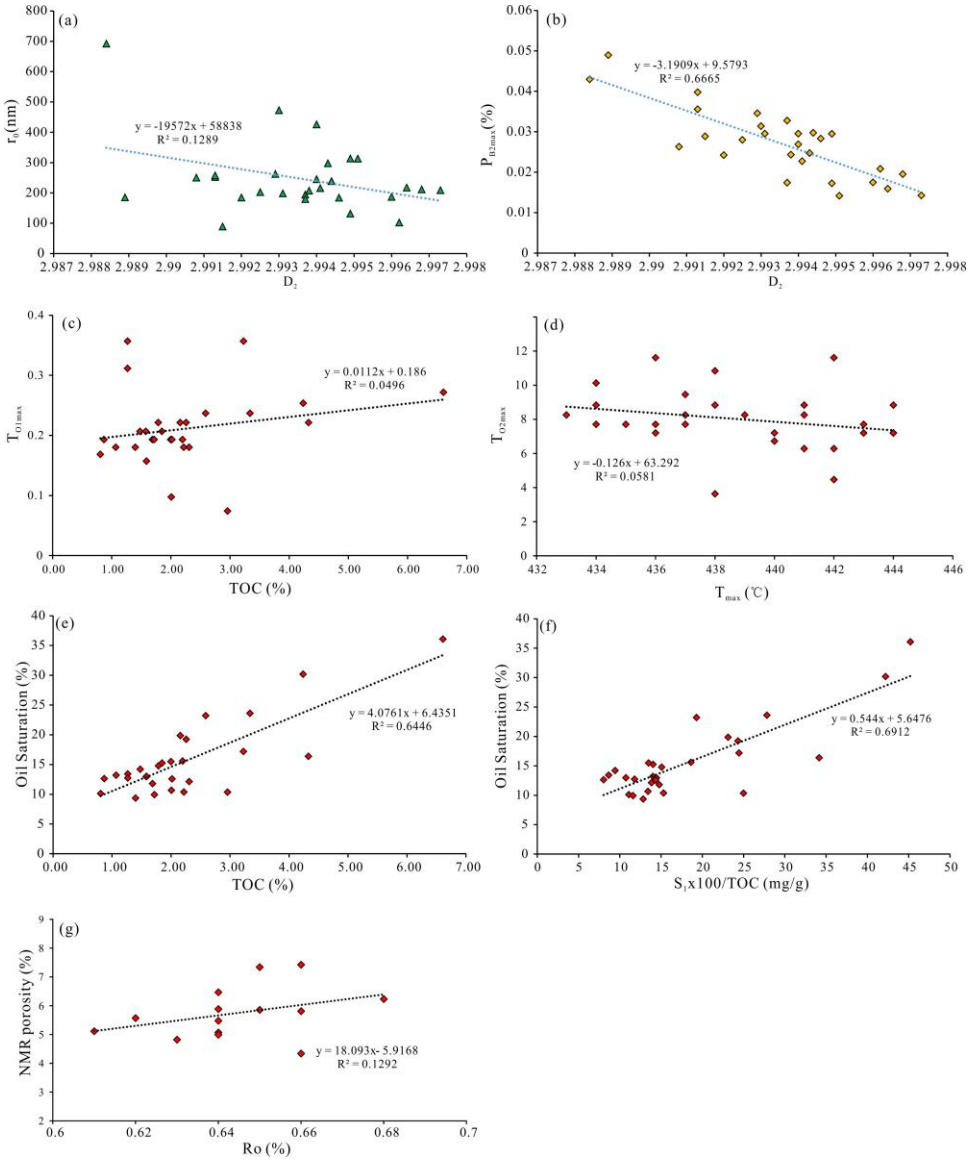

Figure 8. Plots of r_0 vs. D_2 (a) and P_{B2max} vs. D_2 (b) show two negative correlations of fractal dimension (D_2) with the pore size boundary of immovable and movable fluids (r_0) as well as relatively larger pore space. The plots of T_{O1max} vs. TOC content (c) and T_{O2max} vs. T_{max} (d), show a positive correlation between oil viscosity and TOC content, and a negative correlation

between oil viscosity and thermal maturity. The oil saturation show positive correlations with TOC content (e) and S_1×100/TOC (f) for MES shale in Nanpu sag. A positive relation between NMR porosity and Ro (g) indicates shows high thermal maturity promotes the development of pore space in MES shale.

6 Discussion

6.1 Effect Factors of the Shale Pore Structure

The pore structure of the MES shale is slightly different from that of the lacustrine Chang-7 shale in the Ordos Basin in terms of its micropore and macropore portions (Jiang et al., 2016c). For the Chang-7 shale, the mesopores contribute most of the pore space, and the contributions of the micro- and macropores are low. In addition, a large percentage of the pore space is attributed to pore sizes larger than 10 μm for the Chang-7 shale, which is rarely observed in the MES shale. Three factors may lead to these differences, including the thermal maturity, T_2 relaxation mechanism and sample preparation. The thermal maturity of the MES shale is relatively low with a Ro of approximately 0.7%, which is lower than that of the Chang-7 shale in the Ordos Basin with a Ro of 0.91%. The low thermal maturity would lead to undeveloped OM nanopores, as shown in the SEM observation (Fig. 3). In contrast, a higher maturity will facilitate nanopore development in shale sediments, as supported the positive correlation between bulk porosity and Ro (Fig. 8g). Moreover, the pore structure was obtained by using T_2 surface relaxation mechanism. While, the hydrocarbon in smaller nanopore space approach to dead oil in low maturity shale, and the viscosity is really high due to the low maturity. Therefore, the relaxation mechanism in the smaller pore maybe dominated by bulk relaxation (Coates et al., 1999). In addition, the liquid invasion methods used in the previous study of Jiang et al. (2016c) would breake the pore stureture by producing some cracks, which would result in errors in the macropore portions. However, the NMR technique is nondestructive, the macropore portions detected are relatively reliable (Hodgkins and Howard, 1999; Coates et al., 1999).

6.2 Oil Relaxation Mechanisms in the MES Shale

For the oil in low maturity EMS shale, its viscosity is high approaching to 11.03cp (50°C) as drilling tested at 3422.6-3436.2m, which is really higher comparing to the study of Zhao et al. (2019). Therefore, the oil T_2 distributions should be explained by the bulk relaxation in this study. In this study, NMR experiments were performed at 308.15 K (35°C); therefore, the relationship between the oil T_2 relaxation time and viscosity can be described as:

$$T_{2bulk} = 2.20 \times \frac{1}{\eta} \quad (8).$$

Therefore, the oil T_2 relaxation time could be used to describe the volume proportions of the liquids with different viscosities. For the MES shale, the dominate oil viscosity ranges 2-70 cp, followed by 0.1-0.7 cp (Fig. 5d). The drilling tested oil viscosity of 11.03cp takes the large proportion (Fig. 5d) and further powerfully support the reliability of bulk relaxation explanation. Furthermore, the oil viscosity of the MES shale oil is relatively lower than that in the Dongying Sag approximately of 0.8-200 cp (Fig. 5f; Chen et al., 2017).

6.3 Oil Mobility in the MES Shale

For gas, it is not necessary to discuss its mobility, while it is important for oil, especially in shale sediments. The pore structure and liquid properties are two important aspects that should be considered in the study of the mobility of liquids in shale sediments. On the one hand, the position and with of the liquid peaks in the T_2 distribution could reflect their properties (Coates et al., 1999). Heavy oil with a high viscosity would have a shorter T_2 relaxation time compared to light oil with a low viscosity, because the viscosity will greatly affect the polar molecule relaxation behavior in a magnetic field (Coates et al., 1999). Therefore, oil typing could be easy in water-wet rocks according to the moderate peak width and distinct position in the T_2 distribution. For the water-wet MES shale, the generally lower T_{Omax} values implies a relatively higher oil viscosity in the MES shale (Coates et al., 1999). The positive relation between the T_{O1max} value and TOC content (Fig. 8c) implies that shale oil may be more viscous in shale reservoirs with higher TOC contents, which may be related to the adsorption of large surface space from nanopore pores and similar chemical and physical properties between OM and heavy oil or bitumen molecules in low maturity source rock (Sandvik et al., 1992; Li et al., 2019a; 2019b). In addition, the high-viscosity oil may be associated with its low thermal maturity (Fig. 8d). The production of shale oil in the Dongying Sag shows that the shale oil could attain an acceptable productivity when the viscosity is lower than 10 cp (Fig. 5f; Chen et al., 2017). The porosity proportion of the oil with a viscosity lower than 10 cp in the MES shale ranges from 43.33% to 65.12% with an average of 53.66%, showing a relatively good mobility in the MES shale.

On the one hand, pore structure information could also be obtained from the brine saturated T_2 distribution. An interesting phenomenon could be observed in this study: the pore sizes corresponding to T_{B0} are larger than 50 nm, which means that all brine water in the micro- and mesopores as well as in some macropores are immovable in the MES shale samples. Because the brine viscosity (0.2-0.8 cp) is notably lower than that of oil (0.2-1000 cp), the high-viscosity oil cannot move in the pore spaces where brine is immovable (Coates et al., 1999). Therefore, parts macropores of the MES shale is movable. According to the percentages of the micro-, meso- and macropores in Fig. 7, the movable oil in the MES shale does not exceed the macropore percentage of 2.26%-68.97% (avg. 32.74%).

6.4 Shale Oil Potential

Comparing to the main shale oil producing area (Table 3), the geological conditions of MES shale are similar to those of Eocene Hetaoyuan shale sediments, and Ek_2 shale sediments. The maturity of shale oil reservoir in China are commonly relatively low, which are lower than that in overseas. Due to the relatively low maturity, the oil density in MES shale is relatively high, which is similar to that in Qiangjiang shale, Ek_2 shale, Hetaoyuan shale, Lucagou shale. While, all shale oil reservoir company with overpressure except Yanchang shale.The pressure coefficient in MES shale is 1.24-1.41, which is relatively high comparing other shale sediments and provides good condition for the oil flow. Therefore, MES shale has a similar even better geological conditions with other shale oil producing area. In addition, the oil saturation has notable positive correlations with TOC contents as well as with the ratio of $S_1 \times 100/TOC$, as shown in Fig. 8e and 8f. Previous studies suggest that a $S_1 \times 100/TOC$ ratio higher than 100 is the shale oil potential threshold for lacustrine shale (Behar et al., 2003; Jarvie, 2012; Li et al., 2018). Based on the positive relationship in this study (Fig. 8f), this threshold value corresponds to an

oil saturation of 60.05% for the lacustrine shale. In general, sand reservoirs with an oil saturation higher than 40% are regarded as good hydrocarbon-bearing reservoirs. Therefore, the previous threshold is unduly restrictive and unreasonable for the evaluation of the shale oil potential in low maturity lacustrine shale.

Comprehensive analysis shows that the shale oil potential in MES shale at Nanpu sag is very promising with six points: (1) the relation of oil saturation and S_1 value suggest that the evaluation threshold of shale oil potential may be unduly restrictive for the low maturity lacustrine shale sediments; (2) the brittle MES shale has good condition for horizontal well fracturing, which will improve pore structure immensely; (3) the low viscosity oil (<10cp) in the MES shale takes considerable portion, which is beneficial for oil flow in the MES shale; (4) the low maturity MES shale could be heated underground by using the development of in situ conversion process technology (Alpak et al., 2013; 2018; Zhao et al., 2018), which could fortify the hydrocarbon potential and reduce the viscosity to facilitate more hydrocarbon flow; (5) the geological conditions of MES shale are similar to other shale oil producing area; (6) the sampling well is located at a relatively high tectonic position due to ocean constraints, therefore, the MES shale at deeper positions may have a good shale oil potential.

Table 3. The comparison of geological condition for shale oil producing area. The data are form Wang et al., (2019) and Zhao et al., (2018).

Basins/ Depressions	Layers	Ro (%)	Porosity (%)	Thickness (m)	Yields	Density (g/cm^3)	Pressure coefficient
Songliao	Qinshankou	0.5-1.3	1.4-8.7	40-150	1-10.23(m^3/d)	0.82-0.85	1.0-1.2
Jiyang	Shahejie	0.5-1.3	2.0-12.4	100-250	2-110(t/d)	0.67-0.86	1.2-1.9
Nanxiang	Hetaoyuan	0.58-0.74	3.2-7.29	200-600	4.68-28.1(m^3/d)	0.82-0.90	1.2-1.3
Jianghan	Qianjiang	0.41-0.76	1.0-13.0	10-50	1.4-10000(t/d)	0.80-1.05	0.87-2.05
Ordos	Yanchang	0.6-1.1	2.0-12.0	30-70	-23.85(m^3/d)	0.80-0.85	0.7-0.9
Qaidam	Shimengou	0.36-0.66	3.0-10.3	~30	0.5-4(t/d)	N.A.	1.3-1.4
Subei	Funing	0.5-1.3	0.2-6.8	50-500	2-36.83(t/d)	0.81-0.85	1.0-1.1
Junggar	Lucaogou	0.6-1.2	5.45-8.35	100-240	17.9(t/d)	0.87-0.92	1.2-1.5
Santanghu	Lucaogou	0.6-1.1	2.0-12.0	10-100	0.01-22.2(m^3/d)	0.85-0.9	1.0-1.2
Alberta	Cardium	>0.7	N.A.	50-150	20-70(t/d)	0.82-0.85	>1.3
Williston	Bakken	0.6-0.9	5-13.0	5-49	210(t/d)	0.81-0.83	1.2-1.5
Permian	Wolfcamp/Spraberry	0.7-1.7	4-12.0	20-150	80(t/d)	0.78-0.84	1.0-1.4
Gulf	Eagle Ford	0.7-1.4	2-12.0	20-60	200(t/d)	0.82-0.87	1.3-1.8
Denver	Niobrara	0.67-0.95	N.A.	200-450	20.7(m^3/d)	0.825	N.A.
Neuken	Vaca Muerta	0.7-1.3	N.A.	40-150	24.3-81(t/d)	0.80-0.83	1.5-2.3
Cangdong Sag	Ek2	0.45-0.84	1-9.0	200-800	29.6(t/d)	0.87-0.91	1.16-1.18
Nanpu sag	EMS shale	0.62-0.68	4.3-7.4	198.5	N.A.	0.85-0.88	1.24-1.41

7 Conclusions

Based on NMR experiments, the pore structure of the low-maturity MES shale was analyzed, and the oil properties and mobility as well as shale oil potential were further evaluated in this study. The pore space in the low-maturity shale spans nano- to microscale with various pore types, which is dominated by mesopores. The mobile portion is complex and has good self-

similarity with high fractal dimensions. The low porosity relates to the thermal maturity, and a higher maturity facilitates pore space development. The low maturity cause in low free hydrocarbon and oil saturation in MES shale. Considering the high viscosity and the dead oil, the NMR relaxation mechanism in smaller pore space of low-maturity shale is proposed to bulk relaxation. The movable oil with a viscosity lower than 10 cp accounts considerable pore space in the MES shale, and the viscosity is affected by TOC content thermal maturity. Comparing with other shale oil producing areas, MES shale has similar geological conditions with them. It hints a suitable and promising shale oil potential for the brittleness MES shale at low tectonic position of the Nanpu Sag under the technologies of in situ conversion process and hydraulic fracturing. This study also provide a new consideration about the NMR application in shale sediments especially for the low-maturity shale sediments. Not every sedimens is appropriative for the surface relaxation. In the future research, the relaxivity, isolated pore and the bulk relaxation should be taken into account in the study of pore structure of shale sediments by using NMR technology.

Acknowledgments, Samples, and Data

We declare that we have no financial and personal relationships with other people or organizations that can inappropriately influence our work, there is no professional or other personal interest of any nature or kind in any product, service and/or company that could be construed as influencing the position presented in, or the review of, the manuscript entitled. The research data is at https://doi.org/10.5061/dryad.4b8gtht9s. This study was supported by the National Science and Technology Major Project of the Ministry of Science and Technology of China (2016ZX05006-006-001). We would like to express our gratitude to Jidong Oilfield, China National Petroleum Corporation (CNPC), for providing basic geological data. We thanks to the experts of Xiao Liu and Lingjian Meng in the research institute of Jidong Oilfield for their help in this study. We are also grateful for the people who provided sincere comments and assisted in the process of writing this manuscript.

References

Akkutlu, I.Y., Baek, S., Olorode, O.M., Wei, P., Zhang, T., & Shuang, A. (2017). Shale Resource Assessment in Presence of Nanopore Confinement, URTEC-2670808-MS, Unconventional Resources Technology Conference, SPE/AAPG/SEG Unconventional Resources Technology Conference. 24-26 July, (Austin, Texas, USA).

Allen, M.B., Macdonald, D.I.M., Zhao, X., Vincent, S.J., & Brouet-Menzies, C. (1997). Early Cenozoic two-phase extension and late Cenozoic thermal subsidence and inversion of the Bohai Basin, northern China. *Marine and Petroleum Geology*, 14 (7-8), 951-972.

Alpak, F.O., Vink, J.C., Gao, G., & Mo, W. (2013). Techniques for effective simulation, optimization, and uncertainty quantification of the in-situ upgrading process. *Journal of Unconventional Oil and Gas Resources*, 3, 1-14.

Alpak, F.O., & Vink, J.C. (2018). Rapid and accurate simulation of the In-situ Conversion Process using upscaled dynamic models. *Journal of Petroleum Science and Engineering*, 161, 636-656.

Ambrose, R.J., Hartman, R.C., Diaz Campos, M., Akkutlu, L.Y., & Sondergeld, C. (2010). New pore-scale considerations for shale gas in place calculations. In: SPE 131772 Unconventional Gas Conference. *Pittsburgh Pennsylvania*, USA.

Bao, Y., Zhang, L., Zhang, S., Liu, Q., & Zhang, L. (2008). The deep abnormal pressure and the formation of lithologic reservoir in Dongying Sag. *Xinjiang Petroleum Geology*, 29 (5), 585-587.

Bao, Y., Zhang, L., Zhang, J., Li, J., & Li, Z. (2016). Factors influencing mobility of Paleogene shale oil in Dongying Sag, Bohai Bay Basin. *Oil and Gas Geology*, 37 (3), 408-414.

Behar, F., Lewan, M.D., Lorant, F., & Vandenbroucke, M. (2003). Comparison of artificial maturation of lignite in hydrous and nonhydrous conditions. *Organic Geochemistry*, 34 (4), 575-600.

Bustin, R.M., Bustin, A.M.M., Cui, A., Ross, D., & Pathi, V.M. (2008). Impact of shale properties on pore structure and storage characteristics. In: SPE Paper 119892 Presented at the Society of Petroleum Engineers Shale Gas Production Conference in Fort Worth, Texas; November 16-18.

Cao, L., Cao, Y., Jiang, Z., Wu, J., Song, G., & Wang, Y. (2017). Shale oil potential of lacustrine black shale in the Eocene Dongying depression: Implications for geochemistry and reservoir characteristics. *AAPG Bulletin*, 101, 1835-1858.

Chalmers, G.R.L., Bustin, R.M., & Power, I.M. (2012a). Characterization of gas shale pore systems by porosimetry, pycnometry, surface area, and field emission scanning electron microscopy transmission electron microscopy image analyses: examples from the Barnett, Woodford, Haynesville, Marcellus, and Doig units. *AAPG Bulletin*, 96, 1099-1119.

Chalmers, G.R.L., Ross, D.J.K., & Bustin, R.M. (2012b). Geological controls on matrix permeability of Devonian gas shales in the Horn River and liard basins, northeastern british Columbia. Can. *International Journal of Coal Geology*, 103, 120-131.

Chen, D., Pang, X., Wang, Y., Dong, T., Jiang, F., Li, L., Pang, H., Bai, H., Pang, B., Qin, R., & Jiang, H. (2019). Palaeoenvironmental periodisms of middle Eocene terrestrial sediments in Bohai Bay Basin, eastern China, and their implications for organic matter accumulation. *Marine and Petroleum Geology*, 104060.

Chen, W. (2017). Research on the Movability of Shale Oil in Dongying Sag and the Optimization Method of Favorable Zone. *China University of Petroleum master degree thesis*.

Chen, Z., Lavoie, D., Malo, M., Jiang, C., Sanei, H., & Haeri-Ardakani, O. (2017b). A dual-porosity model for evaluating petroleum resource potential in unconventional tight shale plays with application to Utica Shale in Quebec, Canada. *Marine and Petroleum Geology*, 80, 333-348.

Clarkson, C.R., Jensen, J.L., Pedersen, P.K., & Freeman, M. (2012). Innovative methods for flowunit and pore-structure analyses in a tight siltstone and shale gas reservoir. *AAPG Bulletin*, 96 (2), 355-374.

Clarkson, C.R., Solano, N., Bustin, R.M., Bustin, A.M.M., Chalmers, G.R.L., He, L., Melnichenko, Y.B., Radlin, A.P., & Blach, T.P. (2013). Pore structure characterization of North American shale gas reservoirs using USANS/SANS, gas adsorption, and mercury intrusion. *Fuel*, 103, 606-616.

Coates, G.R., Xiao, L., & Prammer, M.G. (1999). NMR logging: principles and applications. Houston: Haliburton Energy Services.

Cohaut, N., Blanche, C., Dumas, D., Guet, J.M., & Rouzaud, J.N. (2000). A small angle X-ray scattering study on the porosity of anthracites. *Carbon*, 38, 1391-400.

Collell, J., Galliero, G., Gouth, F., Montel, F., Pujol, M., Ungerer, P., & Yiannourakou, M. (2014). Molecular simulation and modelisation of methane/ethane mixtures adsorption onto a microporous molecular model of kerogen under typical reservoir conditions. *Microporous and Mesoporous Materials*, 197, 194-203.

Dong, Y., Xiao, L., Zhou, H., & Wang, C.Z. (2010). The Tertiary evolution of the prolific Nanpu Sag of Bohai Bay Basin, China: Constraints from volcanic records and tectono-stratigraphic sequences. *GSA Bulletin*, 122 (3-4), 609-626.

Firouzi, M., Rupp, E.C., Liu, C.W., & Wilcox, J. (2014). Molecular simulation and experimental characterization of the nanoporous structures of coal and gas shale. *International Journal of Coal Geology*, 121, 123-128.

Freeman, J.J., Hofman, J.P., Appel, M., & Perkins, R.B. (1999). Restricted diffusion and internal field gradients paper, SPWLA 40th Annual Logging Symposium Transactions.

Guo, T., Zhang, S., Ge, H., Wang, X., Lei, X., & Xiao, B. (2015). A new method for evaluation of fracture network formation capacity of rock. *Fuel* 140, 778-787.

Hansen, J.P., & Skjeltorp, A.T. (1988). Fractal pore space and rock permeability implications. *Physical review. B, Condensed matter*, 38 (4), 26-35.

Hassan, J. (2012). Pore size distribution calculation from 1H NMR signal and N2 adsorption-desorption techniques. *Physica B Physics of Condensed Matter*, 407 (18), 3797-3801.

Hinai, A., Rezaee, R., Esteban, L., & Laban, M. (2014). Comparisons of pore size distribution: a case from the Western Australian gas shale formations. *Journal of Unconventional Oil and Gas Resources*, 8, 1-13.

Hodgkins, M.A., & Howard, J.J. (1999). Application of NMR Logging to Reservoir Characterization of Low-Resistivity Sands in the Gulf of Mexico1. *AAPG Bulletin*, 83 (1), 114-127.

Hou, H., Shao, L., Li, Y., Jing, Lu, J., Li, Z., Wang, S., Zhang, W., & Wen, H. (2017). Geochemistry, reservoir characterization and hydrocarbon generation potential of lacustrine shales: A case of YQ-1 well in the Yuqia Coalfield, northern Qaidam Basin, NW China. *Marine and Petroleum Geology*, 88, 458-471.

Jarvie, D.M. (2012). Shale resource systems for oil and gas: Part 2-shale-oil resource systems. In: Breyer, J.A. (Ed.), Shale Reservoirs-Giant Resources for the 21st Century. *AAPG Memoir*, 97, 89-119.

Jiang, F., Chen, D., Chen, J., Li, Q., Liu, Y., Shao, X., Hu, T., & Dai, J. (2016a). Fractal analysis of shale pore structure of continental gas shale reservoir in the Ordos Basin, NW China. *Energy & Fuels*, 30 (6), 4676-4689.

Jiang, F., Pang, X., Bai, J., Zhou, X., Li, J., & Guo, Y. (2016b). Comprehensive assessment of source rocks in the Bohai Sea area, eastern China. *AAPG Bulletin*, 100 (6), 969-1002.

Jiang, F., Chen, D., Wang, Z., Xu, Z., Chen, J., Liu, L., Huyan, Y., & Liu, Y. (2016c). Pore characteristic analysis of a lacustrine shale: A case study in the Ordos Basin, NW China. *Marine and Petroleum Geology*, 73, 554-571.

Kleinberg, R.L. (1996). Utility of NMR T_2 distributions, connection with capillary pressure, clay effect, and determination of the surface relaxivity parameter ρ_2. *Magnetic Resonance Imaging*, 14 (7-8), 761-767.

Kleinberg, R.L., & Horsfield, M.A. (1990). Transverse relaxation processes in porous sedimentary rock. *Journal of Magnetic Resonance*, 88, 9-19.

Kleinberg, R.L., & Vinegar, H.J. (1996). NMR properties of reservoir fluids. The. Log. Analyst. 37 (06), 20-32.

Krohn, C.E. (1988). Fractal measurements of sandstones, shales, and carbonates. *Journal of Geophysical Research*, 93 (B4), 3297−3305.

Li, M., Chen, Z., Cao, T., Ma, X., Liu, X., Li, Z., Jiang, Q., & Wu, S. (2018). Expelled oils and their impacts on rock-eval data interpretation, Eocene Qianjiang Formation in Jianghan Basin, China. *International Journal of Coal Geology*, 191, 37-48.

Li, M., Chen, Z., Ma, X., Cao, T., Qian, M., Jiang, Q., Tao, G., Li, Z., & Song, G. (2019a). Shale oil resource potential and oil mobility characteristics of the Eocene-Oligocene Shahejie Formation, Jiyang Super-Depression, Bohai Bay Basin of China. *International Journal of Coal Geology*, 204, 130-143.

Li, M., Chen, Z., Qian, M., Ma, X., Jiang, Q., Li, Z., Tao, G., & Wu, S. (2019b). What are in pyrolysis S1 peak and what are missed? Petroleum compositional characteristics revealed from programed pyrolysis and implications for shale oil mobility and resource potential. *International Journal of Coal Geology*, 103321.

Li, S., Guo, H., Liu, W., Sun, D., & Li, H. (2007). Study on oil saturation recovery on cores by using nuclear magnetic resonance. *Journal of Oil and Gas Technology*, 29 (2), 62-66.

Li, W., Pang, X., Snape, C., Zhang, B., Zheng, D., & Zhang, X. (2019d). Molecular Simulation Study on Methane Adsorption Capacity and Mechanism in Clay Minerals: Effect of Clay Type, Pressure, and Water Saturation in Shales. *Energy & Fuels*, 33 (2), 765-778.

Liu, Y., Yao, Y., Liu, D., Zheng, S., Sun, G., & Chang, Y. (2018). Shale pore size classification: An NMR fluid typing method. *Marine and Petroleum Geology*, 96, 591-601.

Ma, C., Dong, C., Lin, C., Elsworth, D., Luan, G., Sun, X., & Liu, X. (2019). Influencing factors and fracability of lacustrine shale oil reservoirs. *Marine and Petroleum Geology*, 110, 463-471.

Mahrooqi, S.H., Grattoni, C.A., Moss, A.K., & Jing X. (2003). An investigation of the effect of wettability on NMR characteristics of sandstone rock and fluid systems. *Journal of Petroleum Science and Engineering*, 39 (3-4), 389-398.

Mastalerz, M., Schimmelmann, A., Drobniak, A., & Chen, Y. (2013). Porosity of Devonian and Mississippian New Albany Shale across a maturation gradient: Insights from organic petrology, gas adsorption, and mercury intrusion. *AAPG Bulletin*, 97 (10), 1621-1643.

Mosher, K., He, J., Liu, Y., Rupp, E., & Wilcox, J. (2013). Molecular simulation of methane adsorption in micro-and mesoporous carbons with applications to coal and gas shale systems. *International Journal of Coal Geology*, 109-110, 36−44.

Na, J.G., Im, C.H., Chung, S.H., & Lee, K.B. (2012). Effect of oil shale retorting temperature on shale oil yield and properties. *Fuel*, 95, 131-135.

Pu, X. (2019). Major Oil Discovery Made in China's Bohai Bay Basin. *AAPG Explorer*.

Ross, D.J.K., & Bustin, R.M. (2008). Characterizing the shale gas resource potential of Devonian Mississippian strata in the western Canada sedimentary basin: application of an integrated formation evaluation. *AAPG Bulletin*, 92(1), 87-125.

Ross, D.J.K., & Bustin, R.M. (2009). The importance of shale composition and pore structure upon gas storage potential of shale gas reservoirs. *Marine and Petroleum Geology*, 26 (6), 916-927.

Rouquerol, J., Avnir, D., Fairbridge, C.W., Everett, D.H., Haynes, J.M., Pernicone, N., Ramsay, J., Ramsay, D.F., Sing, K.S.W., & Unger, K.K. (1994). Recommendations for the characterization of porous solids. *Pure and Applied Chemistry*, 66, 1739-1758.

Sandvik, E.I., Young, W.A., & Curry, D.J. (1992). Expulsion from hydrocarbon sources: the role of organic absorption. *Organic Geochemistry*, 19, 77-87.

Shao, X., Pang, X., Li, H., & Zhang, X. (2017). Fractal analysis of pore network in tight gas sandstones using NMR method: A case study from the Ordos basin, China. *Energy & Fuels*, 31(10), 10358-10368.

Sharma, A., Namsani, S., & Singh, J.K. (2014). Molecular simulation of shale gas adsorption and diffusion in inorganic nanopores. *Molecular Simulation*, 41, 414-422.

Straley, C., Rossini, D., Vinegar, H.J., Tutunjian, P., & Morriss, C. (1997). Core analysis by low-field NMR. Log. Anal. 38, 84-93.

Wang, M., Guo, Z., Jiao, C., Lu, S., Li, J., Xue, H., Li, J., Li, J., & Chen, G. (2019). Exploration progress and geochemical features of lacustrine shale oils in China. *Journal of Petroleum Science and Engineering*, 178, 975-986.

Xie, X., Krooss, B.M., Littke, R., Amann-Hildenbrand, A., Li, M., Li, Z., Snowdon, L.R., & Mohnhoff, D. (2019). Accessibility and mobility of hydrocarbons in lacustrine shale: Solvent flow-through extraction experiments on Eocene oil shales from Bohai Bay Basin, eastern China. *Organic Geochemistry*, 127, 23-36.

Yao, Y., Liu, D., Che, Y., Tang, D., Tang, S., & Huang, W. (2010). Petrophysical characterization of coals by low-field nuclear magnetic resonance (NMR). *Fuel*, 89 (7), 1371-1380.

Yao, Y., & Liu, D. (2012). Comparison of low-field NMR and mercury intrusion porosimetry in characterizing pore size distributions of coals. *Fuel*, 95, 152-158.

Zhang, H., Huang, H., Li, Z., & Liu, M. (2019). Oil physical status in lacustrine shale reservoirs - A case study on Eocene Shahejie Formation shales, Dongying Depression, East China. *Fuel*, 257, 116027.

Zhao, W., Hu, S., & Hou, L. (2018). Connotation and strategic role of in-situ conversion processing of shale oil underground in the onshore China. *Petroleum Exploration and Development*, 45 (4), 537-545.

Zhao, X., Pu, X., Jiang, W., Zhou L., Jin F., Xiao, D., Fu, L., & Li, H. (2019). An exploration breakthrough in Paleozoic petroleum system of Huanghua Depression in Dagang Oilfield and its significance. *Petroleum Exploration and Development*, 46(4), 651-663.

Zhao, X., Zhou, L., Pu, X., Jin, F., Han, W., Xiao, D., Chen, S., Shi, Z., Zhang, W., & Yang, F. (2018). Geological characteristics of shale rock system and shale oil exploration breakthrough in a lacustrine basin: A case study from the Paleogene 1st sub-member of Kong 2 Member in Cangdong sag, Bohai Bay Basin, China. *Petroleum Exploration and Development*, 45(03), 377-388.

Zheng, H.J., Dong, Y.X., Zhu, G.Y., Wang, X.D., & Xiong, Y. (2007). High-quality source rocks in Nanpu Sag. *Petroleum Exploration and Development*, 34 (4), 385-391.

Zolfaghari, A., Dehghanpour, H., & Xu, M. (2017). Water sorption behaviour of gas shales: II. Pore size distribution. *International Journal of Coal Geology*, 179, 187-195.

Zou, Y.R., Sun, J.N., Li, Z., Xu, X., Li, M., & Peng, P. (2018). Evaluating shale oil in the Dongying Depression, Bohai Bay Basin, China, using the oversaturation zone method. *Journal of Petroleum Science and Engineering*, 161, 291-301.